recycling

MDPI

Article

Impact of Recycled Concrete and Ceramic Fillers on the Performance of Cementitious Systems: Microstructural, Mechanical, and Durability Aspects

Tianjun Han, Diego Aponte *, Susana Valls and Marilda Barra Bizinotto

Department of Civil and Environmental Engineering, Universitat Politècnica de Catalunya (UPC-BarcelonaTech), 08034 Barcelona, Spain; tianjun.han@upc.edu (T.H.); susanna.valls@upc.edu (S.V.); marilda.barra@upc.edu (M.B.B.)

* Correspondence: diego.fernando.aponte@upc.edu

Abstract: Cement production is a major contributor to CO_2 emissions, while construction and demolition waste (CDW) presents growing environmental challenges. The new European standard UNE-EN 197-6 permits the use of recycled concrete fines as partial clinker replacements, providing a regulatory framework for integrating CDW into cementitious systems. This study investigates two CDW-derived fillers, FHH (recycled concrete filler) and FHC (recycled ceramic–concrete mixed filler), as partial substitutes for ordinary Portland cement (OPC). The materials were characterized using XRD, XRF, FTIR, and particle size analysis. Cement pastes and mortars with 10%, 20%, and 30% volume replacements were evaluated for hydration behavior, mechanical performance, and durability. At lower replacement levels, FHC promoted ettringite formation and microstructural refinement, while FHH favored carbonate hydrate development; both fillers also exhibited durability comparable to the control. At higher levels, they maintained satisfactory compressive strength. This study offers critical insights into the integration of CDW-derived fillers into cementitious systems, revealing their potential to significantly reduce clinker consumption while maintaining high mechanical and durability standards.

Keywords: concrete recycled filler; ceramic–concrete mixed filler; hydration behavior; mechanical performance; durability; XRD

check for updates

Academic Editor: Akira Otsuki

Received: 24 March 2025
Revised: 20 May 2025
Accepted: 27 May 2025
Published: 1 June 2025

Citation: Han, T.; Aponte, D.; Valls, S.; Bizinotto, M.B. Impact of Recycled Concrete and Ceramic Fillers on the Performance of Cementitious Systems: Microstructural, Mechanical, and Durability Aspects. *Recycling* **2025**, *10*, 108. https://doi.org/10.3390/recycling10030108

Copyright: © 2025 by the authors. Licensee MDPI, Basel, Switzerland. This article is an open access article distributed under the terms and conditions of the Creative Commons Attribution (CC BY) license (https://creativecommons.org/licenses/by/4.0/).

1. Introduction

The construction industry is at the forefront of environmental challenges, grappling with the dual issues of high carbon dioxide emissions from cement production and the escalating accumulation of construction and demolition waste (CDW) [1,2].

Cement production alone accounts for approximately 8% [2,3] of global CO_2 emissions, primarily due to the energy-intensive clinker manufacturing process and the calcination of limestone [4]. Concurrently, CDW generation exceeds 2 billion tons annually, with a significant portion inadequately managed, resulting in adverse environmental impacts such as resource depletion, habitat destruction, and landfill overuse [5,6]. Addressing these challenges necessitates innovative strategies to enhance sustainability in construction practices.

Among potential solutions, the use of recycled fillers derived from CDW presents a promising approach. As evidenced by the investigations of Ruth, Tokareva, and Li et al. [7–9], these fillers can serve as partial replacements for ordinary Portland cement (OPC), reducing clinker consumption and, consequently, the carbon footprint of cementitious systems.

Traditional supplementary cementitious materials (SCMs), such as fly ash, blast furnace slag, and silica fume, have been extensively studied and widely adopted in both research and industry for their ability to improve the performance and sustainability of cement-based materials [10]. Unlike traditional supplementary cementitious materials (SCMs) that are becoming less available due to shifts in industrial processes, CDW-derived fillers are abundant and underutilized [11–13]. Incorporating these materials into cementitious systems not only offers environmental benefits but also aligns with the principles of circular economy and resource efficiency.

This study focuses on two types of recycled fillers: FHH (recycled concrete filler) and FHC (recycled ceramic–concrete mixed filler). FHH is characterized by its high calcite and dolomite content, which can facilitate the formation of stable carbonate hydrates, contributing to long-term microstructural densification. On the other hand, FHC contains relatively higher gypsum and minor reactive aluminosilicates, such as kaolinite, which influence early hydration reactions and microstructural refinement. These distinct compositions provide an opportunity to explore their roles in hydration dynamics, mechanical performance, and durability in cement-based systems.

Despite the potential of CDW-derived fillers, their application in cementitious materials remains underexplored compared to traditional SCMs [14,15]. Most studies have focused on their physical properties or general pozzolanic activity, often neglecting the detailed mineralogical interactions and hydration mechanisms that occur when these fillers are introduced into cement systems. Moreover, the long-term durability of mortars containing such fillers, particularly under aggressive environmental conditions, requires further investigation to establish their practical feasibility.

To address these gaps, this study employs advanced characterization techniques, including X-ray diffraction (XRD), thermogravimetric analysis (TGA), Fourier-transform infrared spectroscopy (FTIR), X-ray fluorescence (XRF), and particle size distribution (PSD) analysis, to evaluate the properties and performance of FHH and FHC. Cement pastes and mortars with replacement ratios of 10%, 20%, and 30% were analyzed to assess hydration behavior, mechanical properties, and durability indicators such as resistance to carbonation and chloride ingress. By integrating microstructural analysis with macroscopic performance assessments, this research provides a comprehensive understanding of the effects of CDW-derived fillers on cementitious systems.

The findings of this study contribute to the growing body of knowledge on sustainable construction materials by demonstrating the feasibility of FHH and FHC as alternative supplementary cementitious materials. This research not only highlights their potential to reduce OPC consumption and associated carbon emissions but also offers insights into optimizing their utilization to enhance the performance and sustainability of cement-based materials. This work seeks to connect material characterization with practical applications, promoting the use of recycled fillers in mainstream construction and contributing to the development of a more sustainable built environment.

2. Materials and Methodology

2.1. Materials

2.1.1. Cement

This study utilized I 52.5 R cement, supplied by cement manufacturer (Molins, Catalunya, Spain), which conforms to UNE-EN 197-1 [16] standards. This OPC is predominantly composed of clinker, gypsum, and limestone.

2.1.2. Fillers

Two types of recycled fillers produced from construction demolition waste by the Spanish company Adec Global (Catalunya, Spain) were used. The first filler is a recycled concrete filler (FHH), with a calculated density of 2.64 g/cm^3 according to UNE 80103:2013 [17]. The second filler is a recycled ceramic–concrete mixed filler (FHC), with a calculated density of 2.62 g/cm^3 according to UNE 80103:2013. The fineness is one of the most critical parameters in the solid reaction mechanism and has a significant impact on the hydration reaction of cement-based materials.

The particle size distribution determined by laser diffraction is shown in Figure 1. The median particle sizes of OPC, FHH, and FHC were determined to be 13.5 µm, 10.6 µm, and 14.1 µm, respectively. Due to its smaller particle size, FHH exhibits a larger specific surface area, which facilitates better packing and densification within the cementitious system. In contrast, FHC exhibits a slightly lower measured density and a larger particle size. Its coarser particles may influence packing efficiency and potentially lead to increased interparticle porosity in the hardened matrix.

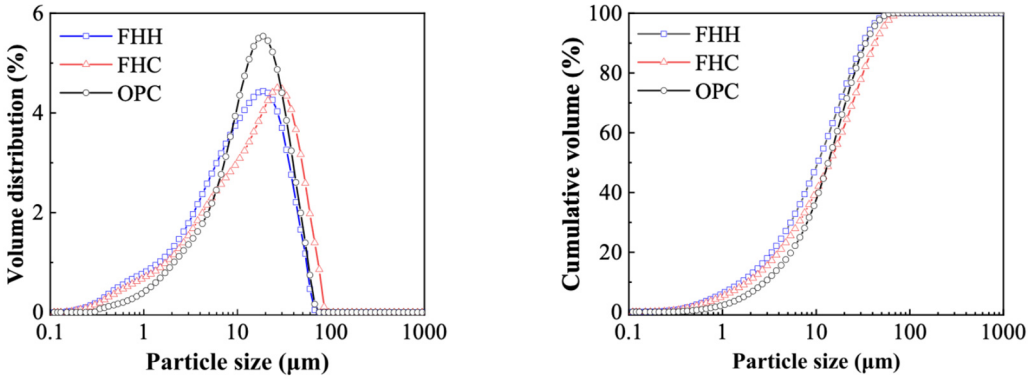


Figure 1. (**a**) Cumulative volume and (**b**) volume distribution of particle size of OPC, FHH, and FHC.

The chemical composition of the samples was determined by X-ray fluorescence (XRF) measurements using a Philips spectrometer, model PW2400 (Philips Analytical, Almelo, the Netherlands), with the results presented in Table 1. As indicated in Table 1, FHH and FHC exhibit similar chemical compositions. Both fillers are characterized by elevated levels of silicon (Si) and aluminum (Al), along with minor amounts of Fe_2O_3, MgO, K_2O, CaO, and SO_3. The aluminosilicate nature of the geopolymeric material is emphasized by the combined SiO_2 and Al_2O_3 content, which accounts for 54.2% in FHH and 58.1% in FHC. However, the CaO content in both FHC and FHH was significantly lower compared to that in conventional cement, being only 13.04% and 18.52%, respectively. It is noteworthy that FHH and FHC contained 0.5% and 1.17% SO_3, respectively. The presence of sulfate ions is likely to significantly influence the hydration reactions in the cement–FHH/FHC system.

Table 1. Chemical compositions of the waste and Portland cement obtained by X-ray fluorescence spectroscopy (in %) (FHH = recycled concrete filler; FHC = recycled ceramic–concrete mixed filler; and OPC = ordinary Portland cement CEM I 52.5 R).

Material	SiO_2	Al_2O_3	Fe_2O_3	CaO	MgO	K_2O	MnO	SO_3	Others	LOI
FHH	47.93	6.25	2.31	18.52	2.82	2.06	0.04	0.5	1.22	18.35
FHC	58.13	8.96	3.2	13.04	1.1	2.53	0.05	1.17	1.68	10.14
OPC	19.96	4.68	3.32	63.27	1.52	0.81	0.03	3.11	0.67	2.63

2.1.3. Sand

These mortars and cement pastes were manufactured using UNE EN 196-1 [18] compliant fine aggregates. The density of the sand was determined following the UNE-EN 1097-6 [19]. For the sand, three different particle densities were determined: oven-dried particle density (d.d) is 2.67 g/cm^3, saturated and surface-dried particle density (s.s.d) is 2.70 g/cm^3, and apparent particle density (a.d) is 2.75 g/cm^3, along with water absorption (w.a) is 1.1%.

2.1.4. Water

The pastes and mortars studied were made using tap water from the laboratory.

2.2. Materials and Experimental Methodology

The research methodology was conducted following the scheme in Figure 2. This study was primarily divided into three phases.

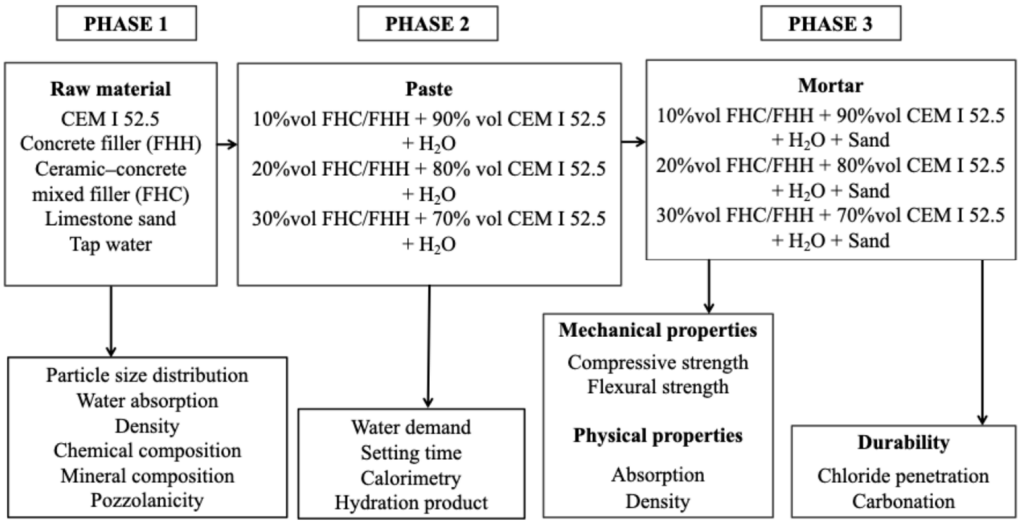


Figure 2. Flowchart of materials and methods.

Phase 1: In the first phase, Fourier-transform infrared spectroscopy (FTIR) and powder X-ray diffraction (XRD) were used to further characterize the raw materials (cement and fillers). The pozzolanic activity of FHH and FHC was evaluated using the UNE-EN 196-5 [20] standard, which assesses chemical reactivity based on the concentrations of calcium and hydroxide ions in solution. The density and water absorption of the sand were determined to understand its suitability for cementitious systems.

Phase 2: In the second phase, paste preparation was initiated, followed by both qualitative analyses. In this experiment, according to UNE-EN 197-6:2023 [21], specific percentages (10%, 20%, and 30%) of FHC and FHH were used to replace an equivalent volume of ordinary Portland cement (OPC) in the paste. The optimal water–binder ratio was determined according to the UNE EN 196-3 [22] by assessing the consistency of the paste at various ratios. Subsequently, the setting time of the paste was measured at this optimal ratio. For both water demand and setting time tests of the FHH/FHC cement pastes, two replicate measurements were performed.

To analyze the impact of fillers on the initial hydration reactions, the semi-adiabatic calorimetry method was employed. The experimental setup consisted of an SQ2020 squirrel data logger from Grant Instrument (Shepreth, UK), connected to a type K thermocouple via its operating software. The thermocouple was inserted into the center of the freshly mixed sample, which was then poured into a sealed and insulated plastic vessel containing 50 g of binding material with the optimal ratio. The plastic vessel was immediately placed

inside an insulated expanded polystyrene container, with a capacity for four samples and one control water sample. Throughout both tests, the room temperature was maintained at approximately 20 °C. The paste samples were hand-mixed externally for less than two minutes, assisted by a vortex mixer directly in the plastic vials, and then loaded into the equipment to measure the heat of hydration and temperature evolution over the first 24 h.

Finally, X-ray diffraction (XRD) was employed to analyze the hydration products formed in the FHH/FHC paste at 7, 28, and 56 days of curing. To prepare the samples for XRD analysis, hydration was stopped by immersing 10 g of crushed FHH/FHC cement paste in ethanol, followed by filtration, drying, and grinding. The overall procedure was carried out with reference to the methodology described in the RILEM TC 238-SCM report [23].

XRD measurements of both raw materials and hydrated samples were conducted using a Bruker D8-A25 diffractometer (Billerica, USA) equipped with a Cu X-ray source (CuKα radiation, 40 kV, and 40 mA) and a LynxEye position-sensitive detector. The scans were performed over a 2θ range of 5° to 65°, with a step size of 0.019° and a counting time of 0.8 s per step. Finally, phase identification was carried out using DIFFRAC.EVA V5.1 software with reference patterns from the ICDD PDF-2 and Crystallography Open Database (COD).

Phase 3: Before preparing the mortar specimens, the consistency of the fresh mortar was evaluated using the flow table method in accordance with UNE-EN 1015-3 [24]. The mortar was placed in a truncated cone mold centered on the flow table, which was dropped 15 times at a controlled rate. The spread diameter was measured in two perpendicular directions to assess workability. Based on these results, a water-to-binder ratio of 0.528 was selected for all mixtures to ensure consistent consistency across tests.

The mortar was prepared according to the standardized procedure described in UNE-EN 196-1, using the mix proportions summarized in Table 2. After preparation, the mortar was poured into oiled 4 × 4 × 16 cm^3 prismatic molds. For each batch of mortar, five molds were prepared, with each mold containing three prismatic samples. Three of these were cured in a humid chamber (95% relative humidity and 20 °C) for 7, 28, and 56 days. After these curing periods, the corresponding microstructural characterization and macroscopic physical and mechanical properties, such as density and water absorption, were determined according to the ASTM C642 [25] standard. The compressive strength was also evaluated according to the UNE-EN 196-1 standard. The remaining two were cured in a humid chamber for 30 days, then cut and waterproofed for testing the carbonation depth and chloride ion penetration depth according to UNE-EN 14630 [26] and NT BUILD 443 [27].

Table 2. Mix proportions of mortar with FHH and FHC as partial cement replacements by volume-based substitution (FHH = recycled concrete filler; FHC = recycled ceramic–concrete mixed filler).

	Substitution Degree (vol.%)	Cement (g)	Filler (g)	Sand (g)	Water (g)	W/B Ratio
FHH	0%	450	0	1350	237.5	0.528
	10%	405	38.2		233.9	
	20%	360	76.4		230.3	
	30%	315	114.6		226.7	
FHC	10%	405	37.9		233.8	
	20%	360	75.8		230	
	30%	315	113.7		226.3	

3. Results and Discussion

3.1. Raw Material Characterization

3.1.1. XRD

The XRD patterns of cement, FHH and FHC are shown in Figure 3. According to the mineral composition determined by XRD, the recycled concrete filler (FHH) and the recycled ceramic–concrete mixed filler (FHC) exhibit very similar mineral phases, primarily consisting of ettringite, albite, biotite, microcline, calcite, quartz, and dolomite. It was observed that FHH contains higher amounts of dolomite and calcite compared to FHC, which is consistent with the higher CaO and MgO contents detected in the XRF analysis (Table 1). In addition, a small gypsum peak and a weak kaolinite peak were identified in FHC, the latter likely originating from ceramic debris present in the recycled waste. As XRD primarily detects crystalline phases, the presence of amorphous content cannot be excluded.

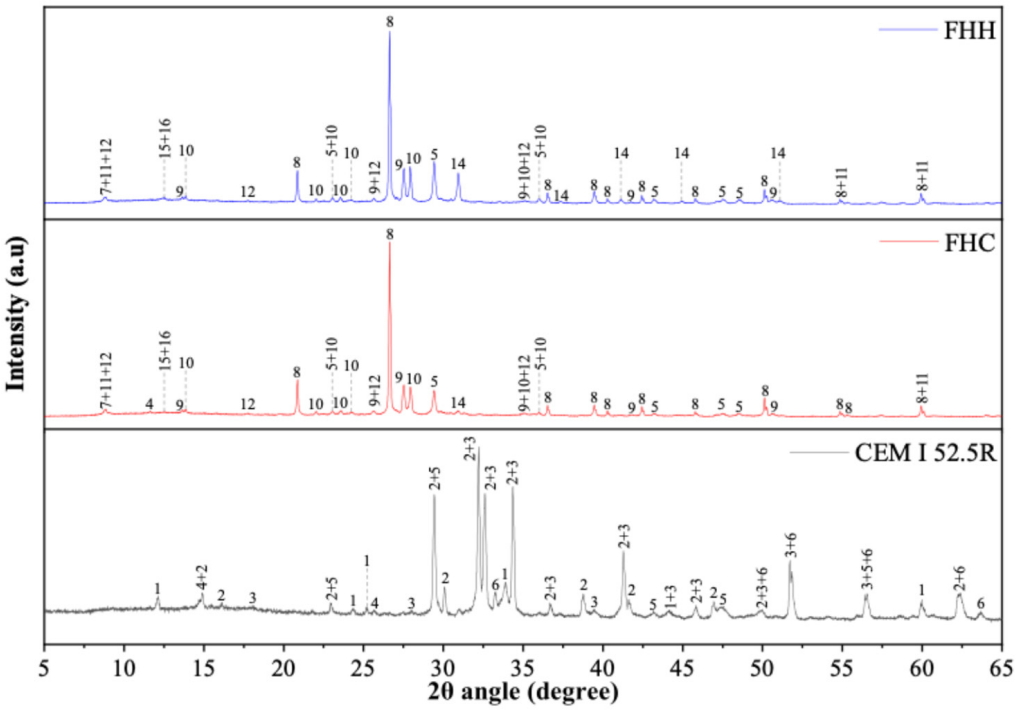


Figure 3. XRD diffractograms of cement, FHH and FHC, where the following are detected: (1) C4AF; (2) C3S; (3) C2S; (4) gypsum; (5) calcite; (6) C3A; (7) ettringite; (8) quartz; (9) microcline; (10) albite; (11) biotite; (12) muscovite; (14) dolomite; (15) kaolinite; and (16) clinochlore.

Gypsum in the cement mortar system can have a significant impact on the hydration reaction. As a primary source of sulfate ions, gypsum reacts with tricalcium aluminate (C_3A) to form ettringite, which regulates the setting time of the cement and prevents flash setting. Additionally, the presence of gypsum may extend the induction period, reducing the early hydration rate and consequently influencing the overall hydration process and the evolution of the microstructure.

3.1.2. FTIR

The FTIR spectra of FHH and FHC, shown in Figure 4, reveal differences in their mineralogical compositions. The characteristic absorption peaks at 713 cm^{-1}, 873 cm^{-1}, and 1420 cm^{-1} correspond to the vibrational modes of carbonate phases, predominantly calcite ($CaCO_3$) and dolomite ($CaMg(CO_3)_2$) [28]. The strongest absorption peak, located at

approximately 1000 cm^{-1}, is attributed to Si-O stretching vibrations from quartz, microcline, albite, and biotite [29], which are present in both FHH and FHC.

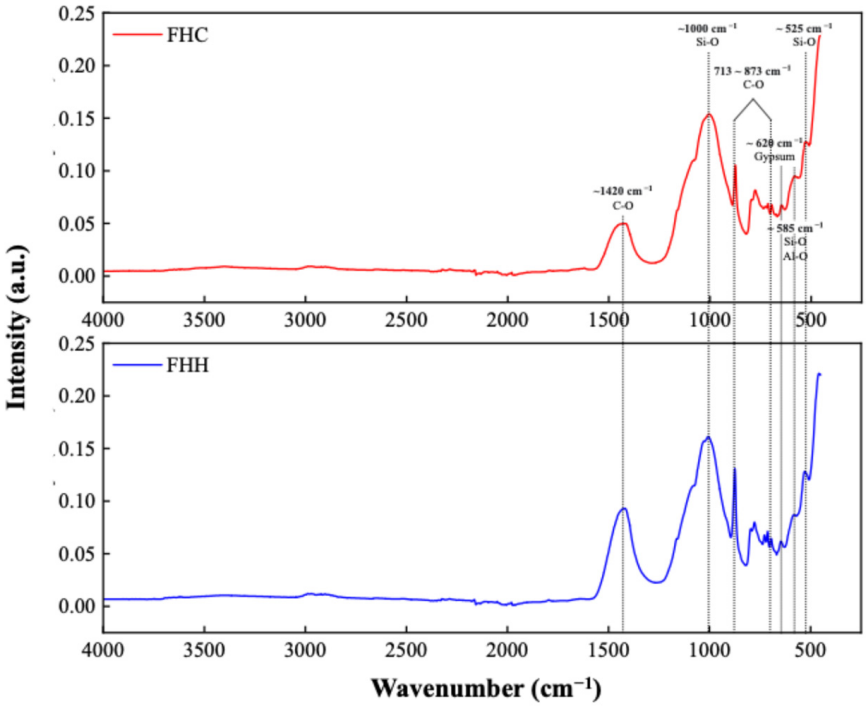


Figure 4. FTIR spectra of FHH and FHC.

A characteristic peak around 620 cm^{-1} appears in both FHH and FHC spectra, commonly attributed to sulfate vibrations in gypsum. However, its precise assignment requires careful consideration, as ettringite (AFt) also exhibits vibrational modes in a similar wavenumber region. XRD analysis confirms the presence of gypsum, supporting its contribution to this peak. The stronger intensity observed in FHC aligns with its higher SO_3 content, as indicated by XRF analysis. The weak or indistinct gypsum peaks elsewhere in the spectrum may be attributed to its low overall content, background absorption from silicate and carbonate phases, or possible interactions with hydration products that influence IR absorption behavior. Peaks at 585 cm^{-1} and 525 cm^{-1} are attributed to the vibrational modes of aluminate and silicate phases, respectively, which likely originate from residual clinker components or secondary hydration products.

These spectral features provide valuable insights into the compositional differences between FHH and FHC and their potential implications for hydration and microstructural development in cement-based systems.

3.1.3. Pozzolanic Activity

Figure 5, based on UNE-EN 196-5, shows the CaO solubility curve at 40 °C and identifies the valid interpreted range of hydroxyl ion concentrations, defined by the standard as 45–90 mmol/L. Figure 5 shows the following: I, the pozzolanic zone, where the measurement point below the solubility curve indicates volcanic ash reactivity and, II, the non-pozzolanic zone, where the measurement point is above the curve or outside the valid $[OH^-]$ range.

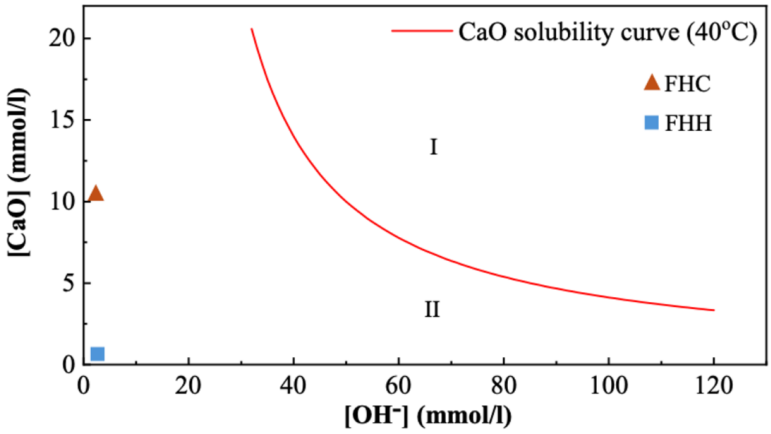


Figure 5. FHH and FHC pozzolanic activity assessment (I: Pozzolanic zone, II: Non-pozzolanic zone).

For FHH, the hydroxide and calcium ion concentrations are 3.20 mmol/L and 1.72 mmol/L, and, for FHC, the values are 2.40 mmol/L and 11.15 mmol/L, respectively, and, since both values are outside of the effective [OH^-] range, neither material is pozzolanic.

3.2. Fresh Properties of FHH/FHC–Cement System

3.2.1. Water Demand

The water demand is primarily related to the specific surface area and the particle size distribution of the filler [30,31]. A larger specific surface area results in higher water demand. The particle size distribution of FHH is smaller than that of FHC, which indicates that FHH has a larger specific surface area compared to FHC.

According to UNE-EN 196-3, the water demand of the FHH/FHC–cement systems was measured, and the results are presented in Figure 6. As the substitution degree of FHH or FHC increases, the water demand initially increases and then decreases. Specifically, the water demand increases from 37.6% at 10% substitution to a peak of 39.5% at 20% substitution for the FHH–cement system and from 37.6% to 39.0% for the FHC–cement system. At a substitution degree of 30%, the values slightly decrease to 38.0% for both systems.

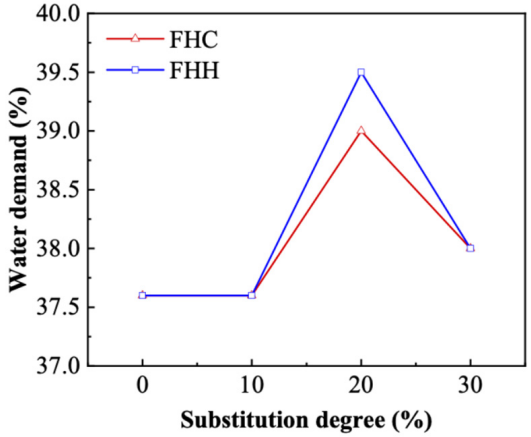


Figure 6. Water demand of cement pastes with different FHH/FHC substitution degrees (by volume).

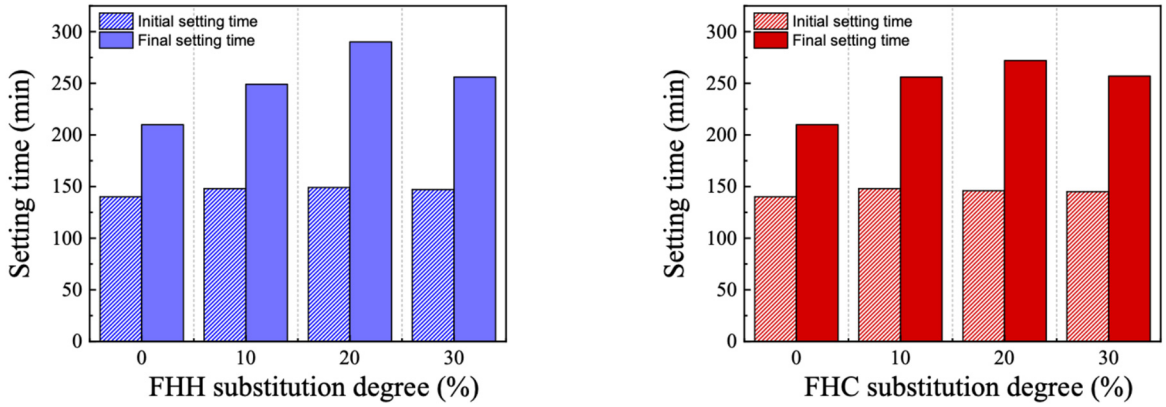
At a substitution degree of 10%, the influence of the filler on water demand is negligible. However, when the substitution degree increases from 10% to 20%, a noticeable rise in water demand is observed, with the FHH–cement paste exhibiting a higher value than the FHC–cement paste. This can be attributed to the finer particle size of FHH (10.6 μm)

compared to FHC (14.1 μm) and OPC (13.5 μm), which results in a larger specific surface area and, thus, a greater amount of water required for wetting and dispersion.

When the substitution degree increased from 20% to 30%, the water demand of both FHH and FHC cement systems decreased slightly from 39.5% and 39.0% to 38.0%, respectively, representing a reduction of approximately 1%. Currently, we do not have a clear explanation for this observation. Further research is required to understand the mechanisms behind this trend.

3.2.2. Setting Time

As shown in Figure 7, the initial and final setting times of fresh FHH/FHC–cement pastes at different substitution ratios of FHH/FHC are presented. The detailed numerical values can be found in Table 3.



(**a**) (**b**)

Figure 7. Initial and final setting time of FHH (**a**) and FHC (**b**) cement pastes with different substitution degrees (by volume).

Table 3. Setting time of FHH/FHC–cement paste (FHH = recycled concrete filler; FHC = recycled ceramic–concrete mixed filler).

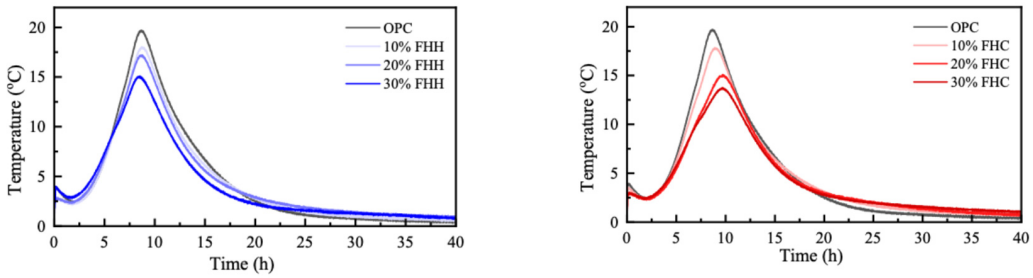
Substitution Degree (vol.%)	Initial Setting Time (min)		Final Setting Time (min)	
	FHH	FHC	FHH	FHC
0%	140	140	210	210
10%	148	148	249	256
20%	149	146	290	272
30%	147	145	256	257

The initial and final setting times of FHH/FHC–cement pastes are prolonged with increasing FHH/FHC substitution ratios. The impact of varying FHH/FHC substitution ratios (10%, 20%, and 30%) on the initial setting time is relatively minor. The addition of FHH increases the initial setting time by approximately 5.71%, while the addition of FHC increases the initial setting time by about 4.52%. The effect of FHH and FHC on the final setting time is more pronounced. At a 10% substitution ratio of FHH/FHC, the final setting time of FHH paste increases by 18.57%, and that of FHC paste increases by 21.90%. At a 20% substitution ratio, the final setting time of FHH paste increases by 38.10%, and that of FHC paste increases by 29.52%. At a 30% substitution ratio, the final setting time of FHH paste increases by 21.90%, and that of FHC paste increases by 22.38%. Since both FHH and FHC are low-reactivity recycled fillers, their addition dilutes the cement clinker, resulting in fewer hydration products formed at early stages. Therefore, the extended

setting time is reasonable [32]. This demonstrates that the addition of FHH and FHC can effectively extend the final setting time of cement pastes. Notably, as the substitution ratio of FHH/FHC increases, the final setting time of the cement paste shows a trend of initially increasing and then decreasing. This is mainly attributed to differences in water demand at varying FHH/FHC substitution ratios.

3.2.3. Semi-Adiabatic Calorimetry

As the amount of FHH substitution ratio increases, the main hydration peak decreases in height and shifts to the left. The reduction in the main hydration peak is attributed to the decreased quantity of cement participating in the hydration reaction due to the increased FHH content. Additionally, the finer particle size of FHH compared to cement and FHC provides more nucleation sites for the precipitation of hydration products, accelerating the hydration reaction and causing the main hydration peak to shift to the left. However, since FHH lacks both cementitious and pozzolanic properties, increasing its substitution ratio at a constant water-to-cementitious material ratio raises the water-to-cementitious material ratio. This dilution effect would typically shift the main hydration peak to the right [33]. Nevertheless, as shown in Figure 8, in the FHH–cement system, the heterogeneous nucleation effect is greater than the dilution effect.



(**a**) (**b**)

Figure 8. Semi-adiabatic calorimetry test results for all studied FHH (**a**) and FHC (**b**) cement samples.

As the substitution ratio of FHC increases, the height of the main hydration peak decreases and shifts to the right. The reduction in the height of the main hydration peak is due to the decreased amount of cement available for the reaction. The rightward shift in the main hydration peak can be attributed to two factors: the dilution effect of FHC and the chemical effect of FHC. Based on the analysis results from XRD, XRF, and FTIR, FHC contains a higher proportion of gypsum. With a constant water-to-binder ratio, increasing the replacement rate of FHC leads to an increased gypsum content in the FHC–cement system. During the early stages of hydration, gypsum dissolves and releases sulfate ions into the pore solution. These sulfate ions adsorb onto the surface of C_3A particles, forming a temporary protective layer and reacting to form ettringite, which suppresses the rapid dissolution of C_3A and thereby prolongs the induction period. An increased sulfate concentration enhances this adsorption effect, further inhibiting aluminate hydration. This mechanism was confirmed in the study by Scrivener and José [34,35]. Additionally, their research showed that sulfate ions also adsorb onto early-formed C–S–H needles. Upon sulfate depletion, these ions are desorbed, triggering renewed C_3A dissolution and the subsequent formation of additional ettringite or transformation into AFm phases. Therefore, the higher gypsum content in FHC increases the availability of sulfate ions in the system, delaying sulfate depletion and extending the induction period for both C_3A and, indirectly, C_3S hydration. In this way, gypsum not only delays aluminate hydration but also modulates the kinetics of silicate hydration.

In summary, the combined effects of the dilution and chemical effects of FHC slow down the formation rate of the primary hydration products in the FHC–cement system, resulting in the delayed appearance of the main hydration peak.

3.2.4. Consistency of FHH/FHC Mortar

Figure 9 shows the consistency results of standardized mortar made by partially replacing cement with FHH/FHC. The results indicate that the use of FHH and FHC as cement replacements leads to a reduction in mortar consistency. At a substitution ratio of 10%, the consistency of FHC mortar showed no significant change compared to the control group, while the consistency of FHH mortar decreased by 3.69%. At a substitution ratio of 20%, the consistency of FHH and FHC mortars decreased by 6.69% and 3.37%, respectively, compared to the control. At a substitution ratio of 30%, the consistency of FHH and FHC mortars decreased by 12.86% and 5.14%, respectively, compared to the control.

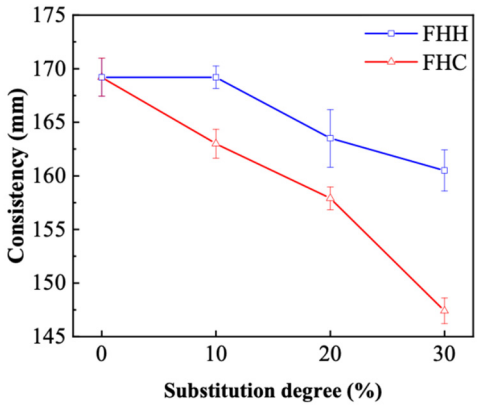


Figure 9. Consistency of FHH and FHC mortars.

It should be noted that, at the same substitution ratio, the consistency of FHH mortar decreases more than that of FHC mortar. This is because FHH has a smaller specific surface area than FHC, leading to stronger water adsorption, which results in relatively less free water in the FHH–cement system. Free water has the most direct impact on mortar fluidity [36,37]: the less free water available, the greater the friction between particles in the mortar, and the lower the consistency.

3.3. Hardened Properties of FHH/FHC–Cement System

3.3.1. Hydration Products of the Cement Pastes

The cement paste was analyzed using XRD to determine the mineralogical changes occurring during hydration due to the addition of FHH and FHC (Figure 10). Across all samples, primary hydration products such as ettringite and portlandite were consistently observed. At 7 days of hydration, hemicarbonate was identified. At 56 days, hemicarbonate peaks disappeared completely, replaced by stronger monocarbonate peaks, particularly at higher replacement levels.

This transformation highlights the influence of calcite and dolomite from FHH and FHC, which serve as sources of carbonate ions, facilitating carbonation processes [38,39]. FHH promotes greater carbonate hydrate formation compared to FHC due to its higher calcite and dolomite content. Concurrently, portlandite peaks show a noticeable reduction at higher replacement levels due to cement clinker dilution.

Non-reactive phases such as quartz, microcline, and albite remained stable throughout the hydration period. Although FHH and FHC primarily act as inert fillers, their mineralogical composition influences the hydration process, leading to changes in portlandite

consumption and the formation of stable carbonate hydrates, particularly at elevated replacement levels.

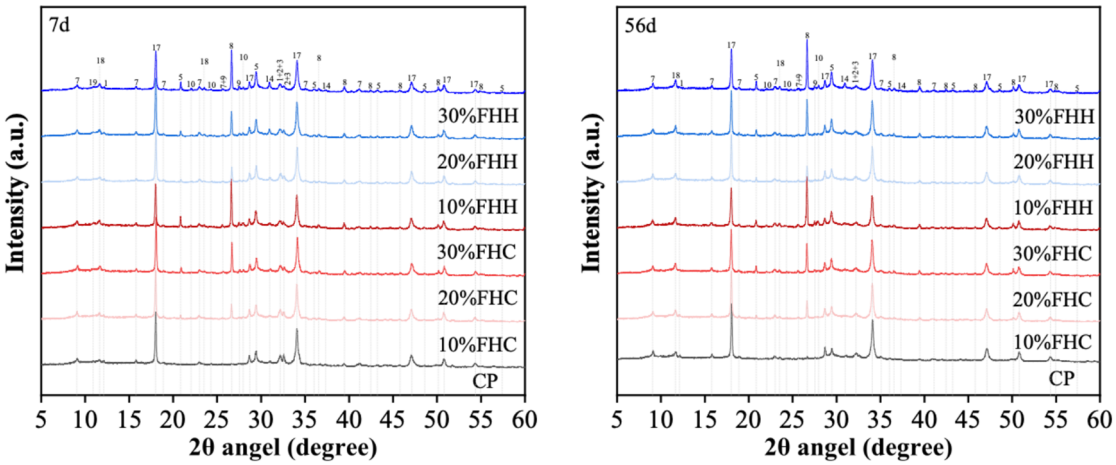


Figure 10. FHH and FHC paste diffractograms at 7 (**a**) and 56 (**b**) curing days: (1) C4AF; (2) C3S; (3) β-C2S; (5) calcite; (7) ettringite; (8) quartz; (9) microcline; (10) albite; (14) dolomite; (15) kaolinite; (16) clinochlore; (17) portlandite; (18) monocarbonate; and (19) hemicarbonate.

3.3.2. Compressive and Flexural Strength

Figures 11 and 12 show the results of the flexural strength and compressive strength tests conducted on FHH/FHC mortar samples after 7, 28, and 90 days of curing, respectively.

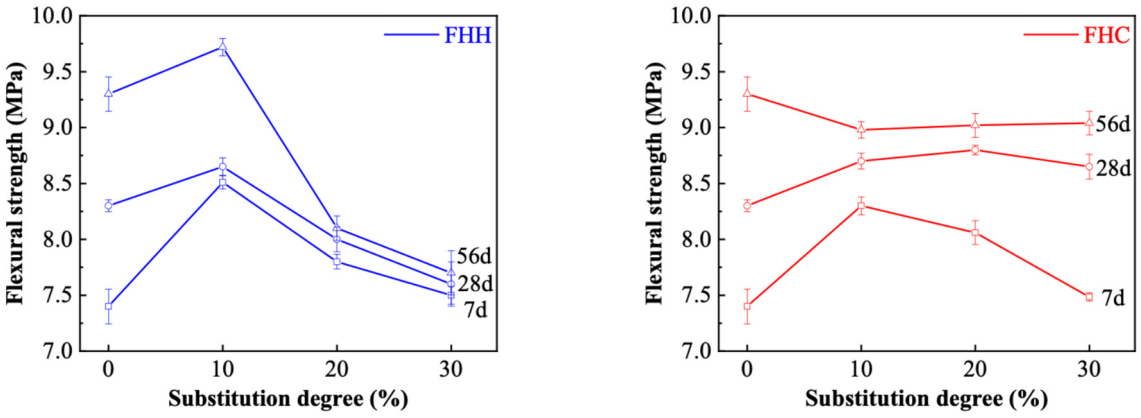
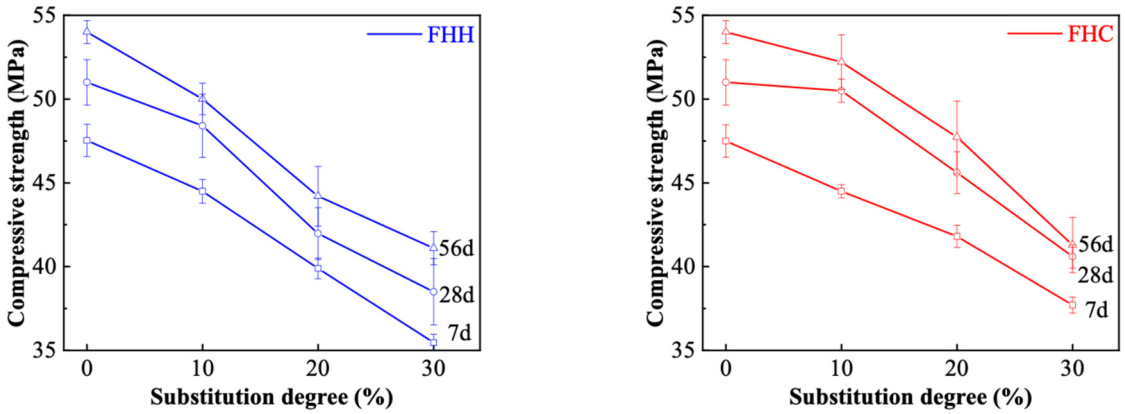


Figure 11. Flexural strength of FHH (**a**) and FHC (**b**) mortars.

From the analysis of flexural strength, after 7 days of curing, the FHH and FHC mortar samples with a 10% substitution ratio showed higher flexural strength compared to the OPC, with FHH mortar samples exhibiting the highest flexural strength at approximately 8.5 MPa, which is about 16.2% higher than the OPC. As the substitution ratio increased, the flexural strength of both FHH and FHC mortars showed a decreasing trend, with the flexural strength dropping to 7.5 MPa for FHH and 7.4 MPa for FHC at a 30% substitution ratio. After 28 days of curing, the flexural strength of FHC mortar samples at different substitution ratios was very similar, around 8.7 MPa, and all were stronger than the control group. For FHH mortar samples, only the 10% substitution ratio showed flexural strength higher than the control. Finally, after 56 days of curing, only the FHH mortar samples with a 10% substitution ratio exhibited flexural strength higher than the control group, with a

strength of approximately 9.8 MPa, and continued to show a growth trend. Meanwhile, the flexural strength of the FHC mortar samples remained almost unchanged compared to the 28-day curing results.



(**a**) (**b**)

Figure 12. Compressive strength of FHH (**a**) and FHC (**b**) mortars.

The reason why FHH mortar with a 10% substitution ratio can achieve better flexural strength compared to the OPC mortar may be attributed to the smaller particle size distribution of FHH, which allows it to mechanically wedge into the cement matrix, which in turn enhances its flexural strength [40–42]. The W/B ratio is also a key factor affecting flexural strength [43]. As mentioned in Section 3.2.4, the addition of FHH reduces the amount of free water in the FHH–cement mortar system, thereby lowering the effective W/B ratio, which in turn enhances the flexural strength.

The compressive strength of both FHC and FHH cement mortars decreased progressively with increasing replacement degrees at all curing ages. At 56 days of curing, FHC mortars showed reductions of 3.3%, 13.0%, and 22.2% for 10%, 20%, and 30% replacement degrees, respectively. The corresponding strength losses for FHH mortars were 7.4%, 18.1%, and 23.9%. At 28 days, FHC mortars exhibited decreases of 1.0%, 8.8%, and 19.4%, while FHH mortars decreased by 2.5%, 21.6%, and 24.5% at the same replacement degrees. Similarly, at 7 days, strength reductions were 6.3%, 12.0%, and 20.6% for FHC, and 6.3%, 16.0%, and 25.3% for FHH.

According to the chemical composition analysis, FHC contains higher amounts of SiO_2, Al_2O_3, and SO_3 compared to FHH. The aluminum in both FHC and FHH is primarily present in feldspar minerals, specifically microcline and albite. As reported by Bagheri [44], feldspar can undergo slow dissolution under highly pH conditions, releasing Al^{3+} ions into the solution, which contributes to the formation of additional AFm phases. As studied by Matschei [45], in the presence of carbonate ions, AFm phases preferentially react with carbonate to form carboaluminate phases, which are more stable and persist in the hydrated matrix.

At low replacement degrees (10%), the gypsum present in FHC promotes the formation of ettringite. As hydration progresses, ettringite gradually transforms into AFm phases. These AFm phases can subsequently react with carbonate (originating either from atmospheric CO_2 or from the partial dissolution of carbonate minerals such as calcite and dolomite present in the FHC and FHH systems) to form hemicarbonate and monocarboaluminate. These carbonate AFm hydrates fill microvoids and densify the matrix, thereby partially offsetting the negative impact of reduced clinker content on the total amount of hydration products and contributing to improved long-term compressive strength.

As the replacement degree exceeds 10%, however, the compressive strength of both FHC/FHH–cement mortars decreases more noticeably. This trend is primarily attributed to the dilution effect, in which increasing the replacement degree reduces the amount of clinker available for hydration. Consequently, the formation of key hydration products (C–S–H and portlandite) is diminished, impairing the strength development of the mortar. While low replacement levels (10%) may compensate for clinker dilution through the enhanced formation of carbonate AFm phases, higher replacement degrees lead to insufficient hydration product formation and, ultimately, a significant reduction in compressive strength.

In addition, since no quantitative analysis was conducted, the presence of amorphous phases in FHH and FHC cannot be excluded. As observed in the compressive strength results, FHC mortars with 10% replacement exhibited a more pronounced strength increase between 28 and 56 days of curing compared to FHH. This delayed strength development may be related to a gradual reaction between amorphous components in the FHC and cement hydration products. However, this hypothesis requires further investigation in future studies to clarify the extent and kinetics of the amorphous phase reactivity.

3.3.3. Density and Absorption

Figures 13 and 14 show the changes in density and water absorption of all FHH/FHC mortar samples over the curing time. The physical properties of all samples exhibit a similar trend: as time progresses, the density of the samples increases, while the water absorption decreases.

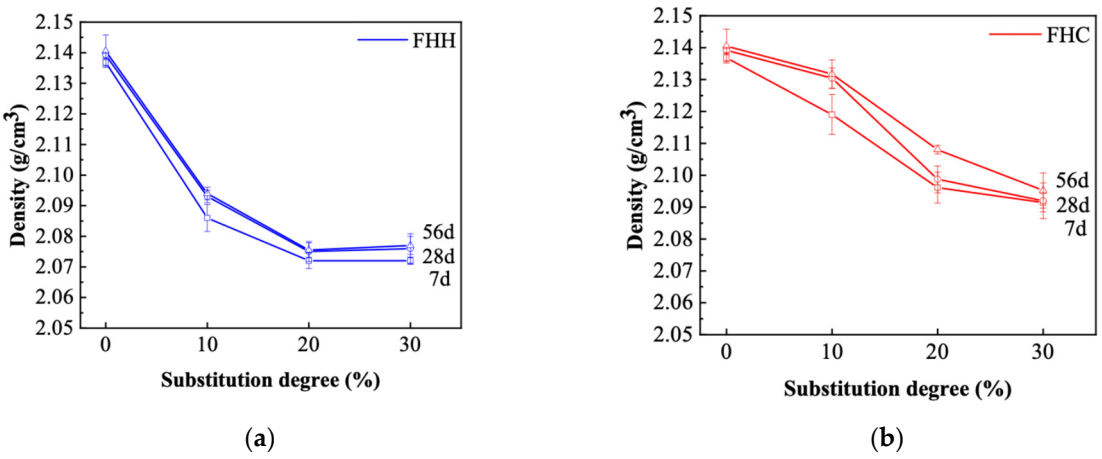


Figure 13. Density of FHH (**a**) and FHC (**b**) mortars.

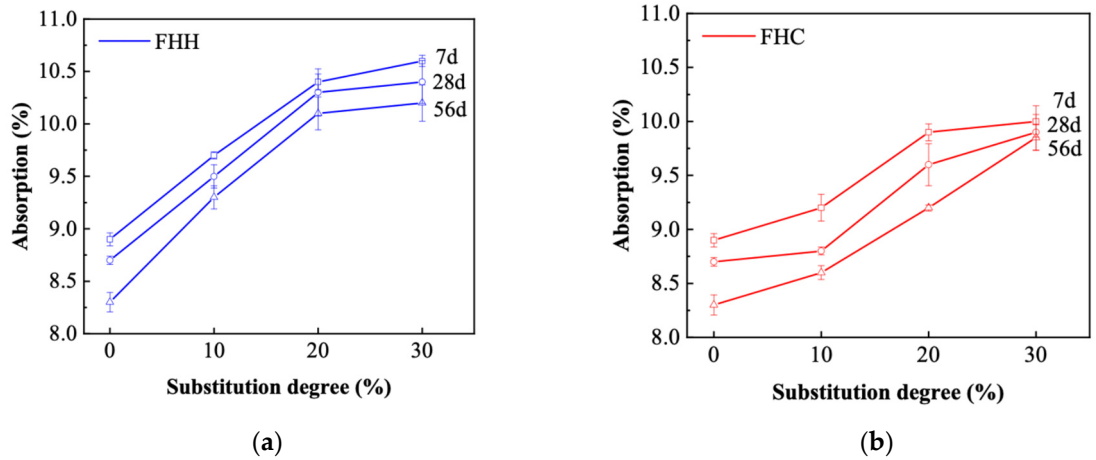


Figure 14. Absorption of FHH (**a**) and FHC (**b**) mortars.

From the 7th to the 56th day of curing, the OPC mortar consistently shows the highest density, with values of 2.137 g/cm^3 and 2.140 g/cm^3 on the 7th and 56th days, respectively. As the substitution ratio increases, the density of the mortars gradually decreases. The density of FHH mortars with 20% and 30% substitution ratios remained very similar throughout the curing period, reaching 2.072 g/cm^3 and 2.073 g/cm^3 on the 7th and 56th days, respectively, corresponding to 96.8% and 97.8% of the OPC mortar density. The closest density to OPC was observed in the FHC mortar with a 10% substitution ratio, which reached 99.0% of the OPC mortar density on the 7th day and 99.4% on the 56th day.

Throughout the curing process, OPC mortar exhibited the lowest water absorption rates. Water absorption increased with higher FHH/FHC replacement rates, but, at the same substitution ratio, FHC mortars consistently showed lower water absorption than FHH mortars. When using 10% FHC to replace cement in the mortar, the initial voids in the system are larger, resulting in lower density compared to OPC due to the dilution effect. However, as hydration progresses, more ettringite and carboaluminate phases are formed in the FHC–cement system [46–48], which have larger volumes that better fill the voids, leading to increased system densification, ultimately reaching a density close to that of OPC mortar.

3.4. Durability

3.4.1. Carbonation

The carbonation coefficient depends on the porosity and permeability of the mortar, as well as the environmental conditions in which it is found. The carbonation coefficient of the mortar can reflect the difficulty for CO_2 to enter the mortar. The higher the carbonation coefficient, the easier it is for CO_2 to enter the mortar. Conversely, the more difficult it is for CO_2 to enter the mortar.

The carbonation experiment was conducted on mortar specimens cured for 28 days, following the standardized procedure outlined in UNE-EN 14630. The carbonation depth of the specimens was recorded after 30, 60, and 90 days of carbonation. By substituting the measured carbonation depth data into the following Equation (1), the carbonation coefficient can be calculated:

$$X = K \times \sqrt{t} \quad (1)$$

where X, K, and t represent the carbonation depth (mm), the carbonation coefficient of the mortar, and CO_2 exposure time (days).

Through the calculation, we obtain the carbonation depth as a function of time (Figure 15). From Figure 15 and Table 4, it can be seen that, as the substitution ratio of FHH and FHC increases, the carbonation coefficient of the recycled mortars continuously rises. This is due to the dilution effect, which leads to a reduction in hydration products (CH, C-S-H, etc.) and an increase in mortar porosity. Among the samples, the control mortar exhibited the lowest carbonation coefficient, at 1.27. At a 10% replacement rate, the carbonation coefficient of FHH mortar was slightly lower than that of FHC mortar, at 1.42 and 1.49, respectively. At a 20% replacement rate, the carbonation coefficients of FHH and FHC mortars were 2.77 and 1.90, showing a significant difference. Compared to the 10% replacement rate, the carbonation coefficient of FHH mortar increased by 95%, while the carbonation coefficient of FHC mortar increased by 27%. At a 30% replacement rate, the carbonation coefficient of FHH mortar remained the highest among all mortar samples, reaching 3.49.

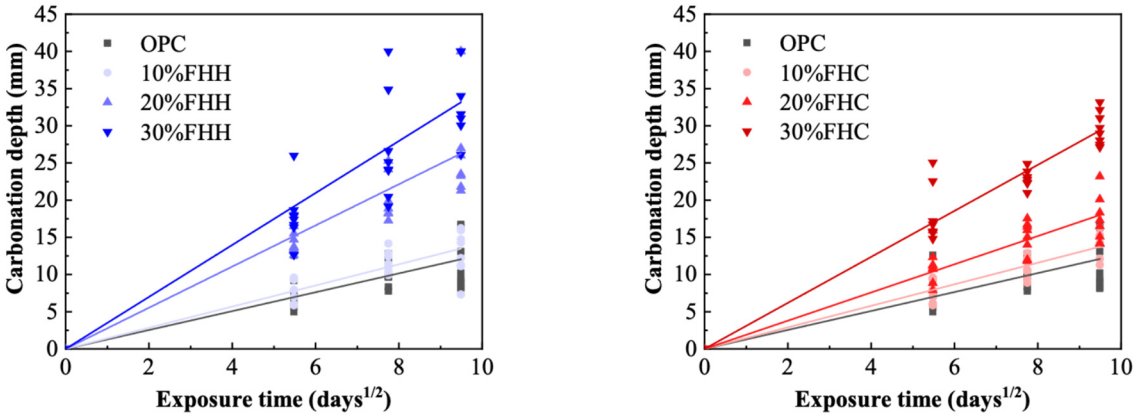


Figure 15. Carbonation depths of FHH (**a**) and FHC (**b**) samples as functions of the square root of carbonation time.

Table 4. Carbonation and penetration coefficients of mortar (FHH = recycled concrete filler; FHC = recycled ceramic–concrete mixed filler).

Substitution Degree (vol.%)	Coefficient of Carbonation (K)		Coefficient of Penetration (D)	
	FHH	FHC	FHH	FHC
0%	1.27	1.27	2.49	2.49
10%	1.42	1.49	2.47	2.51
20%	2.77	1.90	2.97	2.90
30%	3.49	3.09	3.53	3.26

The carbonation of mortar primarily involves the carbonation of CH and C-S-H, with calcite and silica gel as the main carbonation products [49,50]. These products can fill the pores in the mortar, reducing the carbonation coefficient. Compared to FHH, FHC contains more Al_2O_3 and SO_3, resulting in the formation of more sulfoaluminate (AFm, AFt) phases in the FHC–cement mortar system. Sulfoaluminates can react with part of the intruding CO_2 to form carboaluminates, which have a larger volume and help densify the mortar, slowing further carbonation and reducing the carbonation coefficient. Therefore, at the same replacement rate, the carbonation coefficient of FHC mortar is smaller than that of FHH mortar.

3.4.2. Penetration

The diffusion coefficient (D) is an intrinsic property of the mortar. The lower the D value, the more difficult it is for the chloride to penetrate the mortar. When the concentration of the aqueous chloride solution in contact with the mortar is kept constant, the diffusion coefficient D can be calculated through Equation (2):

$$X = 4 \times \sqrt{(D \times t)} \quad (2)$$

where X, D, and t represent the chloride penetration depth (mm), chloride diffusion coefficient of the mortar, and time of exposure to Cl^- (days).

Chloride penetration tests were conducted using mortar specimens cured for 28 days, following the standard procedure outlined in NT BUILD 443. The chloride penetration depth of the specimens was recorded after immersion in a sodium chloride solution (165 g NaCl/L H_2O) for 30, 60, and 90 days. The experimental results are shown in Figure 16. From Figure 16 and Table 4, we can observe that, with the increase in the substitution

ratios of FHH and FHC, the penetration coefficient of recycled fillers gradually increases. This is expected, as the incorporation of FHH and FHC reduces the amount of cement, leading to a decrease in hydration products, which results in an increase in mortar porosity and the penetration coefficient. At a 10% substitution ratio, the penetration coefficients of FHH and FHC mortars are 2.47 and 2.51, respectively, while the penetration coefficient of the control group is 2.49, showing minimal differences among the three. However, as the substitution ratio increases, the penetration coefficient of FHH mortar exhibits a more rapid upward trend. At a 30% substitution ratio, the penetration coefficient of FHH mortar reaches 3.53, the highest among all samples. In a chloride environment, monosulfate (AFm) reacts with the intruding chloride to form Friedel's salt, which slows down the rate of penetration [51,52]. FHH contains fewer alumina phases compared to FHC, and, thus, as the substitution ratio increases, the penetration coefficient of FHH mortar increases more rapidly.

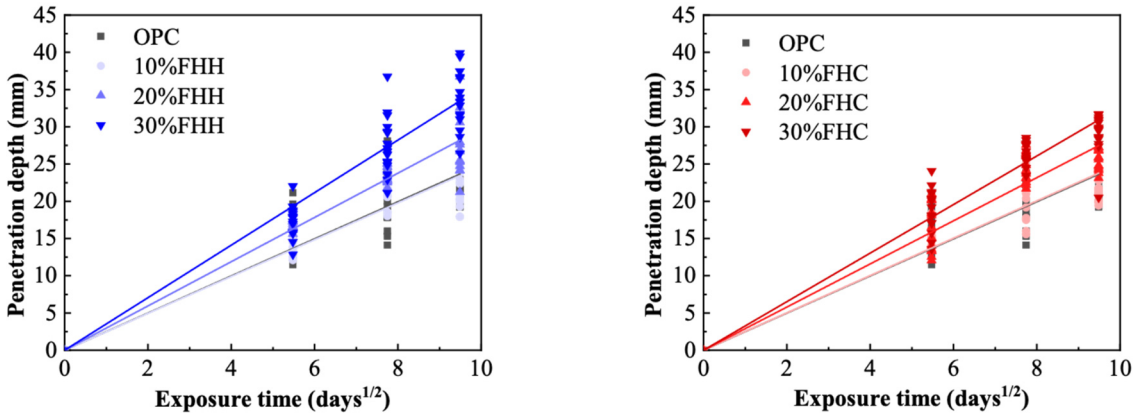


Figure 16. Penetration depths of FHH (**a**) and FHC (**b**) samples as functions of the square root of exposure time.

4. Conclusions

This study examined the use of two recycled fillers, FHH and FHC, as partial cement replacements in cementitious systems. The findings demonstrate that, although these materials are not pozzolanic, their physical and mineralogical characteristics affect hydration, strength, and durability.

1. FHC enhanced ettringite formation and promoted carboaluminate phases, resulting in improved matrix densification. FHH, with higher calcite and dolomite content, led to more extensive carbonate hydrate formation. These reactions explain the different hydration behaviors observed and their influence on mechanical properties.
2. At a 10% replacement level, the compressive strength of FHC–cement systems reached approximately 54 MPa at 56 days, comparable to OPC, indicating suitability for structural use. FHH, while slightly lower in strength, showed higher early-age flexural strength due to its finer particle size and better dispersion, making it appropriate for repair mortars or early-strength applications. However, increasing the replacement ratio exceeded 20% reduced strength in both systems due to clinker dilution and decreased hydration product formation.
3. XRD and FTIR analyses confirmed the formation of secondary hydrates and a reduction in portlandite content, particularly in FHH systems. These results indicate that, although FHH exhibits limited chemical reactivity, it contributes to microstructural development through both physical filler effects and partial carbonate-based reactions.

In contrast, the microstructural refinement in FHC systems was more pronounced, likely due to its higher alumina and sulfate contents, which facilitated the formation of dense AFm phases. These features translated into improved durability: in both chloride penetration and carbonation tests, the FHC–cement systems with 10% replacement demonstrated significantly lower ingress rates. This suggests strong potential for FHC in aggressive environments, such as marine or chloride-rich conditions.

4. These results suggest that FHH and FHC can be effectively used as partial cement replacements at appropriate substitution levels. Their performance depends not only on the replacement level but also on their mineral composition, particle size, and interaction with cement hydration. From an engineering perspective, FHC is viable for partial replacement in structural elements under exposure, while FHH is better suited for non-structural or early-strength applications.

This research highlights the potential of recycled fillers (FHH and FHC) as sustainable alternatives to supplementary cementitious materials (SCMs). Future studies should explore further optimization of these materials, such as fine-tuning particle size or combining with other SCMs, to enhance their performance and broaden their applicability in cementitious systems.

Author Contributions: Formal analysis, investigation, methodology, visualization, writing—original draft, T.H.; conceptualization, formal analysis, methodology, resources, writing—review and editing, D.A.; formal analysis, resources, writing—review and editing, S.V.; conceptualization, project administration, resources, supervision, M.B.B. All authors have read and agreed to the published version of the manuscript.

Funding: This research received no external funding.

Data Availability Statement: The data presented in this study are available upon request from the corresponding author due to university ownership rights.

Acknowledgments: The first author would like to thank the China Scholarship Council (CSC No. 202408390003). Additionally, Diego Aponte participates in the Serra Húnter fellow program.

Conflicts of Interest: The authors declare no conflicts of interest.

Abbreviations

The following abbreviations are used in this manuscript:

CDW	Construction and demolition waste
FHH	Recycled concrete filler
FHC	Recycled ceramic–concrete mixed filler
FTIR	Fourier transform infrared spectroscopy
XRD	X-ray diffraction
XRF	X-ray fluorescence
PSD	Particle size distribution

References

1. Gao, T.; Shen, L.; Shen, M.; Liu, L.; Chen, F. Analysis of material flow and consumption in cement production process. *J. Clean Prod.* **2016**, *112*, 553–565. [CrossRef]
2. Kajaste, R.; Hurme, M. Cement industry greenhouse gas emissions—Management options and abatement cost. *J. Clean Prod.* **2016**, *112*, 4041–4052. [CrossRef]
3. Andrew, R.M. Global CO_2 emissions from cement production. *Earth Syst. Sci. Data* **2018**, *10*, 195–217. [CrossRef]
4. Desport, L.; Andrade, C.; Corral, D.; Selosse, S. Feasibility, conditions, and opportunities for achieving net-negative emissions in the global cement industry. *Int. J. Greenh. Gas Control.* **2025**, *141*, 104280. [CrossRef]
5. Ding, Z.; Wang, Y.; Zou, P.X.W. An agent based environmental impact assessment of building demolition waste management: Conventional versus green management. *J. Clean Prod.* **2016**, *133*, 1136–1153. [CrossRef]

6. Butera, S.; Christensen, T.H.; Astrup, T.F. Life cycle assessment of construction and demolition waste management. *Waste Manag.* **2015**, *44*, 196–205. [CrossRef]
7. Oliveira, D.R.B.; Leite, G.; Possan, E.; Filho, J.M. Concrete powder waste as a substitution for Portland cement for environment-friendly cement production. *Constr. Build. Mater.* **2023**, *397*, 132382. [CrossRef]
8. Tokareva, A.; Kaassamani, S.; Waldmann, D. Fine demolition wastes as Supplementary cementitious materials for CO_2 reduced cement production. *Constr. Build Mater.* **2023**, *392*, 131991. [CrossRef]
9. Li, J.; Deng, X.; Lu, Z.; Li, X.; Hou, L.; Jiang, J.; Yang, F.; Zhang, J.; He, K. Recycled concrete fines as a supplementary cementitious material: Mechanical performances, hydration, and microstructures in cementitious systems. *Case Stud. Constr. Mater.* **2024**, *21*, e3575. [CrossRef]
10. Henríquez, P.A.; Aponte, D.; Ibáñez-Insa, J.; Bizinotto, M.B. Ladle furnace slag as a partial replacement of Portland cement. *Constr. Build Mater.* **2021**, *289*, 123106. [CrossRef]
11. Liu, X.; Li, J.; Bai, C.; Peng, R.; Chi, Y.; Liu, Y. Optimum low-carbon transformation pathways of China's iron and steel industry towards carbon neutrality based on a dynamic CGE model. *Energy* **2024**, *313*, 134023. [CrossRef]
12. Bhardwaj, N.; Seethamraju, S.; Bandyopadhyay, S. Carbon abatement options for large iron and steel plants in India. *J. Clean Prod.* **2025**, *486*, 144505. [CrossRef]
13. Yan, Y.; Pang, Y.X.; Luo, X.; Lin, Q.; Pang, C.H.; Zhang, H.; Gao, X.; Wu, T. Carbon dioxide-focused greenhouse gas emissions from petrochemical plants and associated industries: Critical overview, recent advances and future prospects of mitigation strategies. *Inst. Chem. Eng.* **2024**, *188*, 406–421. [CrossRef]
14. Snellings, R.; Suraneni, P.; Skibsted, J. Future and emerging supplementary cementitious materials. *Cem. Concr. Res.* **2023**, *171*, 107199. [CrossRef]
15. Juenger, M.C.G.; Snellings, R.; Bernal, S.A. Supplementary cementitious materials: New sources, characterization, and performance insights. *Cem. Concr. Res.* **2019**, *122*, 257–273. [CrossRef]
16. *UNE-EN 197-1*; Cement—Part 1: Composition, Specifications and Conformity Criteria for Common Cements. AENOR: Madrid, Spain, 2011.
17. *UNE 80103*; Test Methods of Cements. Physical Analysis. Actual Density Determination. AENOR: Madrid, Spain, 2013.
18. *UNE-EN 196-1*; Methods of Testing Cement—Part 1: Determination of Strength. AENOR: Madrid, Spain, 2018.
19. *UNE-EN 1097-6*; Test for Mechanical and Physical Properties of Aggregate—Part 6: Determination of Particle Density and Water Absorption. AENOR: Madrid, Spain, 2014.
20. *UNE-EN 196-5*; Methods of Testing Cement—Part 5: Pozzolanicity Test for Pozzolanic Cement. AENOR: Madrid, Spain, 2011.
21. *UNE-EN 197-6*; Cement—Part 6: Cement with Recycled Building Materials. AENOR: Madrid, Spain, 2023.
22. *UNE-EN 196-3*; Methods of Testing Cement—Part 3: Determination of Setting Times and Soundness. AENOR: Madrid, Spain, 2016.
23. Snellings, R.; Chwast, J.; Cizer, Ö.; De Belie, N.; Dhandapani, Y.; Durdzinski, P.; Elsen, J.; Haufe, J.; Hooton, D.; Patapy, C.; et al. RILEM TC-238 SCM recommendation on hydration stoppage by solvent exchange for the study of hydrate assemblages. *Mater. Struct. Mater. Constr.* **2018**, *51*, 172. [CrossRef]
24. *UNE-EN 1015-3*; Methods of Test for Mortar for Masonry—Part 3: Determination of Consistence of Fresh Mortar (by Flow Table). AENOR: Madrid, Spain, 2000.
25. *ASTM C642-13*; Standard Test Method for Density, Absorption, and Voids in Hardened Concrete. ASTM International: West Conshohocken, PA, USA, 2013.
26. *UNE-EN 14630*; Products and Systems for the Protection and Repair of Concrete Structures, Test methods, Determination of Carbonation Depth in Hardened Concrete by the Phenolphthalein Method. AENOR: Madrid, Spain, 2007.
27. *NT BUILD 443*; Concrete Hardened: Accelerated Chloride Penetration. Nordtest: Espoo, Finland, 1995.
28. Ji, J.; Ge, Y.; Balsam, W.; Damuth, J.E.; Chen, J. Rapid identification of dolomite using a Fourier Transform Infrared Spectrophotometer (FTIR): A fast method for identifying Heinrich events in IODP Site U1308. *Mar. Geol.* **2009**, *258*, 60–68. [CrossRef]
29. Jiang, L.; Zheng, H.; Xiong, J.; Fan, Z.; Shen, T.; Xie, H.; Chen, M.; Li, J.; Gu, Z.; Li, H.; et al. Fabrication of negative carbon superhydrophobic self-cleaning concrete coating: High added-value utilization of recycled powders. *Cem. Concr. Compos.* **2023**, *136*, 104882. [CrossRef]
30. Aiqin, W.; Chengzhi, Z.; Ningsheng, Z. The theoretic analysis of the influence of the particle size distribution of cement system on the property of cement. *Cem. Concr. Res.* **1999**, *29*, 1721–1726. [CrossRef]
31. Mehdipour, I.; Khayat, K.H. Effect of particle-size distribution and specific surface area of different binder systems on packing density and flow characteristics of cement paste. *Cem. Concr. Compos.* **2017**, *78*, 120–131. [CrossRef]
32. Zhang, H.; Zhang, C.; He, B.; Yi, S.; Tang, L. Recycling fine powder collected from construction and demolition wastes as partial alternatives to cement: A comprehensive analysis on effects, mechanism, cost and CO_2 emission. *J. Build. Eng.* **2023**, *71*, 106507. [CrossRef]

33. Wang, D.; Shi, C.; Farzadnia, N.; Shi, Z.; Jia, H.; Ou, Z. A review on use of limestone powder in cement-based materials: Mechanism, hydration and microstructures. *Constr. Build. Mater.* **2018**, *181*, 659–672. [CrossRef]
34. Scrivener, K.; Ouzia, A.; Juilland, P.; Mohamed, A.K. Advances in understanding cement hydration mechanisms. *Cem. Concr. Res.* **2019**, *124*, 105823. [CrossRef]
35. Da, J.; Neto, S.A.; De La Torre, A.G.; Kirchheim, A.P. Effects of Sulfates on the Hydration of Portland Cement—A Review. *Constr. Build. Mater.* **2021**, *279*, 122428.
36. Klemczak, B.; Gołaszewski, J.; Cygan, G.; Gołaszewska, M.; Jonkers, H.; Zhilyaev, D.; Koenders, E.A. Utilization of waste foam concrete with MPCM as a substitution material for cement in mortars. *J. Build. Eng.* **2024**, *90*, 109284. [CrossRef]
37. de M, T.D.; Nunes, U.S.; Marinho, G.S.; de O, J.C.; Martinelli, A.E.; da Nóbrega, A.C.V. Limestone calcined clay cement (LC^3) coating mortars as an energy-efficient option for construction. *Constr. Build. Mater.* **2024**, *437*, 136954. [CrossRef]
38. Caneda-martínez, L.; Monasterio, M.; Moreno-juez, J.; Martínez-ramírez, S.; García, R.; Frías, M. Behaviour and properties of eco-cement pastes elaborated with recycled concrete powder from construction and demolition wastes. *Materials* **2021**, *14*, 1299. [CrossRef]
39. Krishnan, S.; Bishnoi, S. Understanding the hydration of dolomite in cementitious systems with reactive aluminosilicates such as calcined clay. *Cem. Concr. Res.* **2018**, *108*, 116–128. [CrossRef]
40. Çelik, D.N.; Demircan, R.K.; Shi, J.; Kaplan, G.; Durmuş, G. The engineering properties of high strength mortars incorporating juniper seed ash calcined at different temperatures: Comparison with other SCMs. *Powder Technol.* **2023**, *422*, 118474. [CrossRef]
41. Culcu, M.B.; Esen, H. Investigation of mechanical, durability, and thermal properties of sustainable self-compacting mortars containing construction demolition waste and supplementary cementitious materials. *J. Build. Eng.* **2024**, *95*, 110361. [CrossRef]
42. Sabrin, R.; Shahjalal, M.; Bachu, H.A.E.; Habib, M.M.L.; Jerin, T.; Billah, A.M. Recycling of different industrial wastes as supplement of cement for sustainable production of mortar. *J. Build. Eng.* **2024**, *86*, 108765. [CrossRef]
43. Zhang, H.; Li, Q.F.; De Zhou, H.; Song, Z.M. Experimental Study and Prediction Model of the Flexural Strength of concrete Containing Fly Ash and Ground Granulated Blast-Furnace Slag. *Adv. Civ. Eng.* **2021**, *2021*, 8773664. [CrossRef]
44. Bagheri, M.; Lothenbach, B.; Shakoorioskooie, M.; Scrivener, K. Effect of different ions on dissolution rates of silica and feldspars at high pH. *Cem. Concr. Res.* **2022**, *152*, 106644. [CrossRef]
45. Matschei, T.; Lothenbach, B.; Glasser, F.P. The AFm phase in Portland cement. *Cem. Concr. Res.* **2007**, *37*, 118–130. [CrossRef]
46. Tang, J.; Li, Z.; Yu, C.; Yu, J. Viability of using recycled powder from CDW to produce ternary cement type LC3. *Case Stud. Constr. Mater.* **2024**, *21*, e3668. [CrossRef]
47. Li, M.; Zheng, K.; Chen, L.; Prateek, G.; Zhou, X.; Yuan, Q. Using metakaolin to improve properties of aged Portland cement: Effectiveness and the mechanism. *Constr. Build. Mater.* **2024**, *428*, 136299. [CrossRef]
48. Bonavetti, V.L.; Rahhal, V.F.; Irassar, E.F. Studies on the carboaluminate formation in limestone filler-blended cements. *Cem. Concr. Res.* **2001**, *31*, 853–859. [CrossRef]
49. Piasta, W. Analysis of carbonate and sulphate attack on concrete structures. *Eng. Fail. Anal.* **2017**, *79*, 606–614. [CrossRef]
50. Zajac, M.; Skibsted, J.; Durdzinski, P.; Haha, M.B. Effect of alkalis on products of enforced carbonation of cement paste. *Constr. Build. Mater.* **2021**, *291*, 123203. [CrossRef]
51. Ekolu, S.; Solomon, F.; Rakgosi, G. Chloride—Induced delayed ettringite formation in Portland cement mortars. *Constr. Build. Mater.* **2022**, *340*, 127654. [CrossRef]
52. Xu, Q.; Ji, T.; Yang, Z.; Ye, Y. Steel rebar corrosion in artificial reef concrete with sulphoaluminate cement, sea water and marine sand. *Constr. Build. Mater.* **2019**, *227*, 116685. [CrossRef]

Disclaimer/Publisher's Note: The statements, opinions and data contained in all publications are solely those of the individual author(s) and contributor(s) and not of MDPI and/or the editor(s). MDPI and/or the editor(s) disclaim responsibility for any injury to people or property resulting from any ideas, methods, instructions or products referred to in the content.